Supporting Information

Ferroelectricity in Un-Doped ZnO Nanorods

Jon Maiz[†,▽], Pauline Loxq[‡], Pierre Fau[‡], Katia Fajerwerg[‡], Myrtil L. Kahn[‡], Guillaume Fleury[†], Georges Hadziioannou[†], Guillaume Guegan[‖], Jérôme Majimel[§], Mario Maglione[§], Vincent Rodriguez[,±], Eleni Pavlopoulou[*,†]*

[†] Laboratoire de Chimie des Polymères Organiques (LCPO-UMR 5629), Bordeaux INP / Université de Bordeaux / CNRS, 16 Av. Pey-Berland, 33607 Pessac, France

[‡] Laboratoire de Chimie de Coordination (LCC – UPR8241), CNRS, 205 route de Narbonne, 31077, Toulouse Cedex 4, France

[‖] ST Microelectronics, 37100 Tours, France

[§] CNRS, Univ Bordeaux, Bordeaux INP, ICMCB, UMR 5026, F-33608 Pessac, France

[±] Institut des Sciences Moléculaires (ISM – UMR5255), Université de Bordeaux/CNRS, 351 cours de la Libération, 33405 Talence Cedex, France

Second Harmonic Scattering Measurements (SHS)

1. Experimental Setup

Figure S1 shows a schematic representation of the setup used for the SHS measurements. The 1064 nm vertically polarized output of a passively mode-locked Nd:YVO4 laser (EKSPLA) producing trains of 65 ps, ≤ 50 μJ pulses at a repetition rate of 2 kHz was used in all experiments. The intensity of the incident beam was controlled by a motorized half-wave plate followed by a Glan-Laser polarizer with its transmission axis fixed vertically. The incident beam average power was less than 30 mW for all experiments.

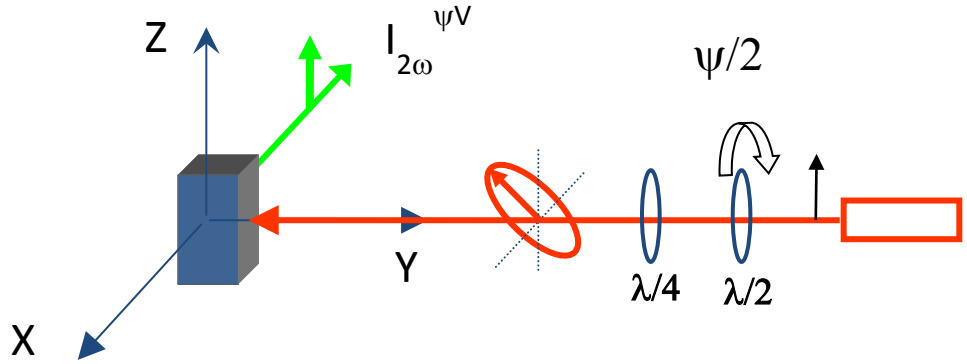

Figure S1. Schematic representation of the right-angle scattering geometry used in the SHS measurements. Before being slightly focused in the liquid sample, the incident fundamental light at 1064 nm can either be vertically (V) polarized or circularly (left (LC)/right (RC)) polarized using a combination of a rotating half-wave plate (λ/2) and a fixed quarter-wave plate (λ/4). The generated second harmonic light at 532 nm scattered at 90° is collected by a lens and analyzed vertically (V) by a polarizer before being filtered and detected.

The laser beam was focused down to a spot size of ~8 μm by a near-infrared objective lens (378-822-5, 5× M Plan Apo, Mitutoyo; numerical aperture 0.14, working distance 37.5 mm) in a 10 mm path fused silica cuvette (117-204-10-40, Hellma) containing the liquid solution. To minimize eventual light absorption of the harmonic scattered beam, the (incident) beam waist was positioned to pass at a distance of 1-2 mm from the inside of the cell wall facing the collecting lens. The generated second harmonic light (532 nm) scattered at 90° was collected by a camera lens (f/1.2, Nikon), analyzed vertically (V), filtered from the fundamental light, and focused into a

spectrograph (Induram, Horiba Jobin Yvon) before being dispersed by a 1800 grooves/mm grating onto a liquid N_2-cooled, back-illuminated CCD camera (Symphony, Horiba; 2048×512 pixels). The power and polarization state of the incident beam as well as the settings of the power and polarization scans were controlled by a custom-designed LabView interface. This setup has been previously described in References 25 and 28.

2. Methods

The polarization configuration was set to vertical-vertical (VV), *i.e.*, with vertically polarized incident light and vertically analyzed scattered light. First of all, the solvent's (THF, HPLC grade) SHS response was measured as a function of the incident power, I^{ω} (Figure S2). A clear quadratic dependence is obtained, in accordance with the 1st term of Eq.1 that describes the solvent's contribution. Pure chloroform was also measured (Figure S2) and used as the reference for the calibration of THF, following the procedure detailed in Ref. 28 for pure liquids. The coefficient of the quadratic dependence that is thus calculated for THF is $C_{THF}\left[\left|\beta\right|^2 C_{VV}\right]_{THF} = 219\,\mathrm{mol\,L^{-1}\,(at.unit)^2}$. Note that this procedure does not require to determine separately β_{SHS} and DR for THF. This coefficient is subtracted from the SHS intensities recorded for the solvent/NPs binary systems in order to isolate the NPs SHS responses.

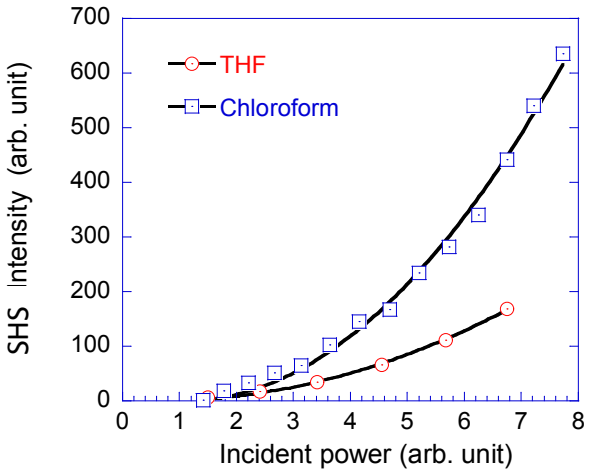

Figure S2. SHS quadratic dependences on the incident power, measured for pure THF and pure chloroform. These data were used for the calibration of THF *vs* chloroform.

Concerning the solvent/NPs solutions, the SHS amplitude can be obtained by performing first a power scan, *i.e.*, a scan of the scattered intensity analyzed vertically, $I_{VV}^{2\omega}$ as a function of the incident intensity, I^{ω}. This measurement allows determining the coefficients of the quadratic dependence of $I_{VV}^{2\omega}$ on I^{ω} , based on Eq.1. These coefficients are obtained by fitting the power curves as a function of the incident power I^{ω} and the NPs concentration C_{NPs}, using a custom-built 2D fitting function of the form:

$$I_{VV}^{2\omega}(I^{\omega},C_{\mathrm{NPs}}) = (|p_1| + |p_2|C_{\mathrm{NPS}})(I^{\omega} - p_3)^2 \qquad \text{(S1)}$$

where p_i (i =1–3) are the fitting parameters. The 3D representations of the $I_{VV}^{2\omega}$ SHS response of all ZnO NP as a function of the incident power and concentration are reported in Figures S4-S9.

The depolarization ratio, *DR*, is obtained by performing a polarization scan, *i.e.*, through a stepwise variation of the polarization state of the incident light, at a fixed incident power. The polarization configuration is set to Ψ-V for the incident and scattered beams respectively, where Ψ is the variable angle of the half-wave plate. Polarization scans are performed for Ψ values between 0° and 360° by 5° steps, typically on the most concentrated solutions. All experiments described herein were carried out at room temperature. Each data point of the polarization scan results by averaging three accumulations with an acquisition time of 20 s each. In order to extract solely the NPs contribution to the polarization scans, it is necessary to measure the scattered intensity from the binary solution for a chosen NP concentration as well as that from the pure solvent (THF) and then subtract the latter from the former (see Eq.1). The NPs *DR* value is determined by fitting the NPs polarization curve (see Figure S3) using a constrained custom-built fitting function of the form (Ref. 25):

$$I_{\Psi V}^{2\omega} = A\left[\cos^4(\Psi - \Psi_0) + B\sin^2(\Psi - \Psi_0)\cos^2(\Psi - \Psi_0) + DR\sin^4(\Psi - \Psi_0)\right] \qquad \text{(S2)}$$

where the amplitude A is a coefficient that contains the fixed I^{ω}, Ψ_0 is an instrumental parameter called the angular offset, B and *DR* are the fitting parameters. In the general case where incoherent (Eq. 2b) and coherent contributions (Eq. 2c) arise, the fitted parameter B is related to *DR* and the coherent contribution Δ^{Coh} through the equation $B = (7 - DR) + \Delta^{Coh}$. Note that this equation is

specific to the setup used herein. For all nanoparticles examined herein, *i.e.* NP1-6, we found $\Delta^{Coh} \approx 0$ within the experimental errors, indicating no coherent contribution. Their SHS polar plots (Figures S4-S9) exhibit a two-lobes feature, intermediate to the pure dipolar/octupolar features reported in Figure S3 (left). (Note that Fig. S6 bottom corresponds to Fig. 2b).

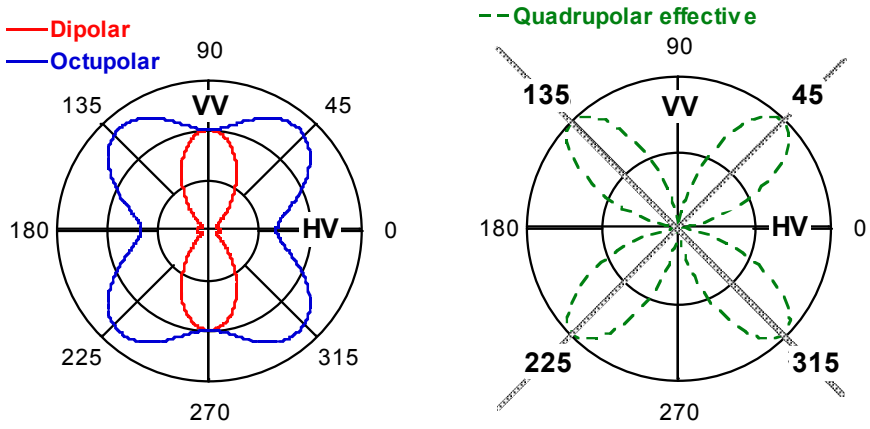

Figure S3. Incoherent (left) and coherent (right) normalized SHS polar plot, according to Eq.2b and Eq.2c, respectively.

3. Data

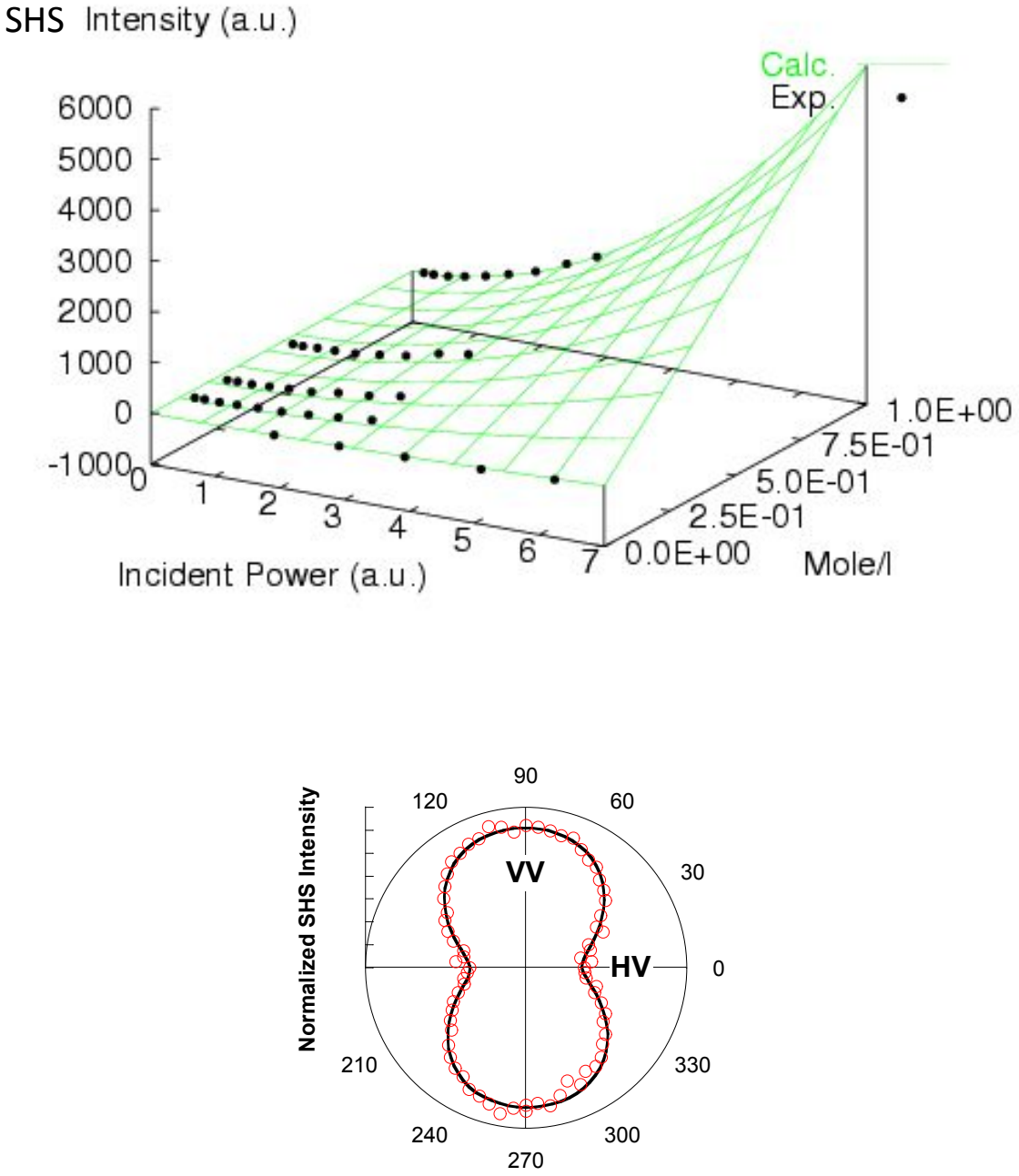

Figure S4. SHS responses of NP-1 in THF. Top: 3D representation of the SHS response as a function of the incident power and NPs concentration. Bottom: Extracted polar plot of the polarization curve of the dispersed ZnO NP-1.

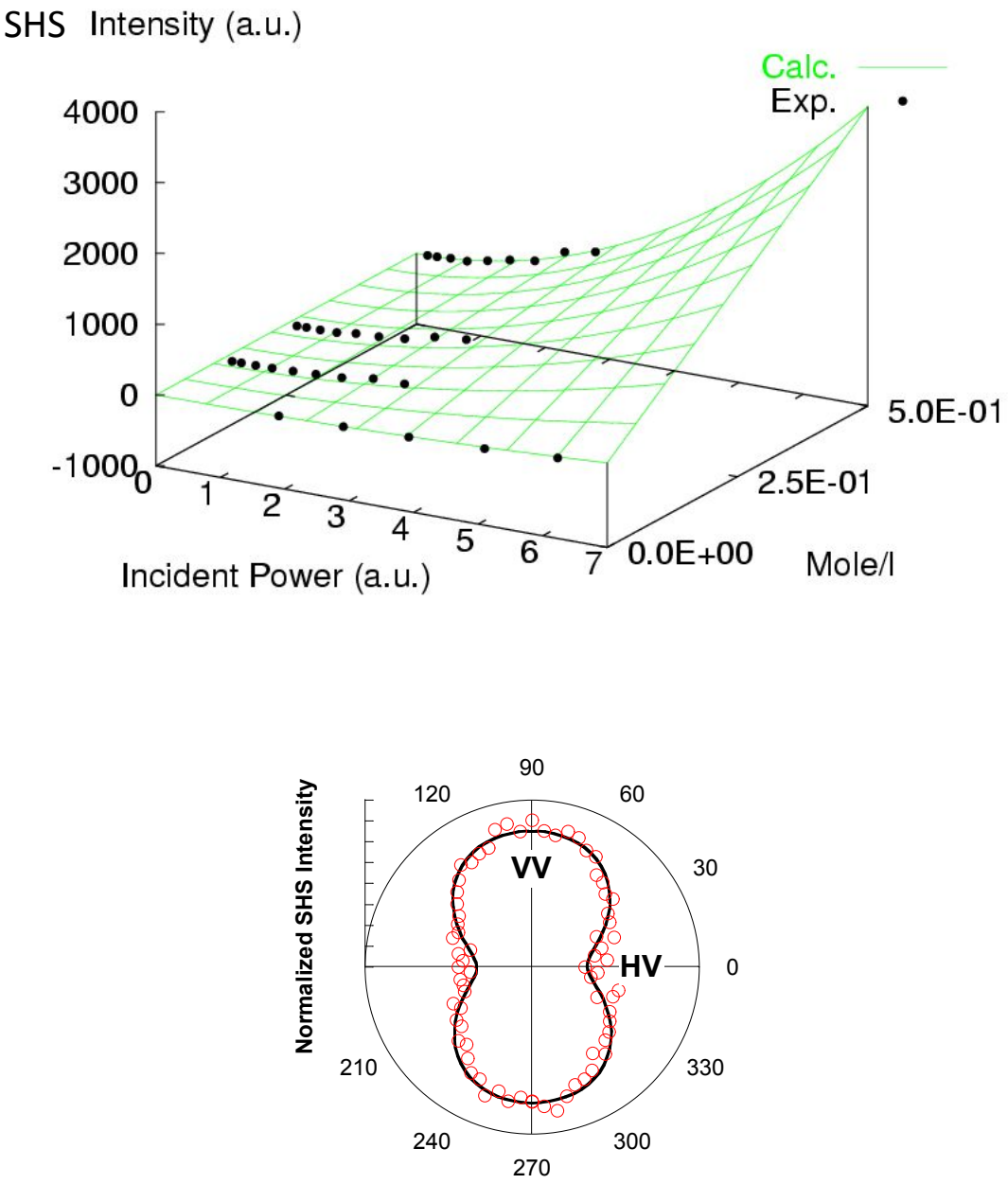

Figure S5. SHS responses of NP-2 in THF. Top: 3D representation of the SHS response as a function of the incident power and NPs concentration. Bottom: Extracted polar plot of the polarization curve of the dispersed ZnO NP-2.

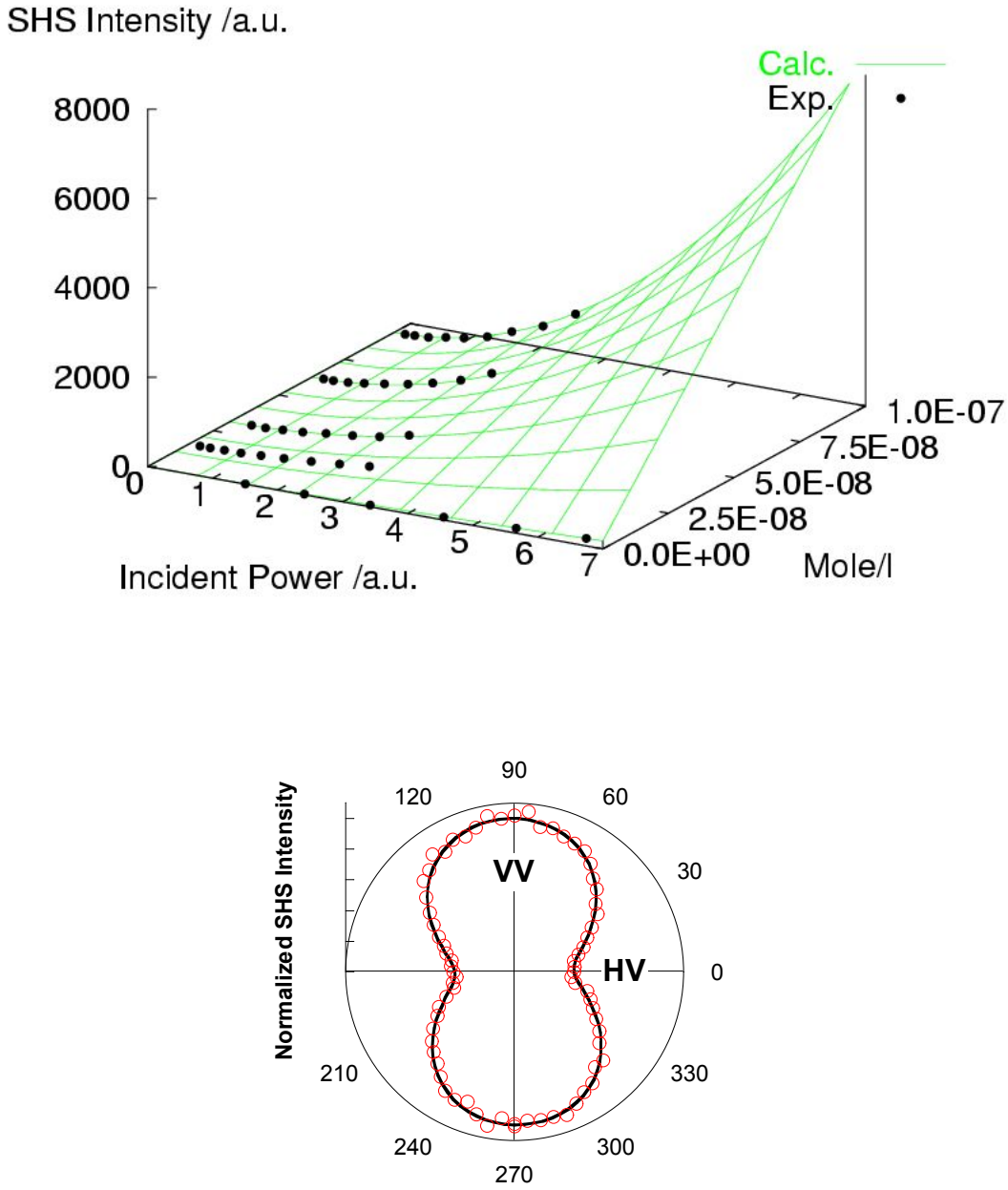

Figure S6. SHS responses of NP-3 in THF. Top: 3D representation of the SHS response as a function of the incident power and NPs concentration. Bottom: Extracted polar plot of the polarization curve of the dispersed ZnO NP-3.

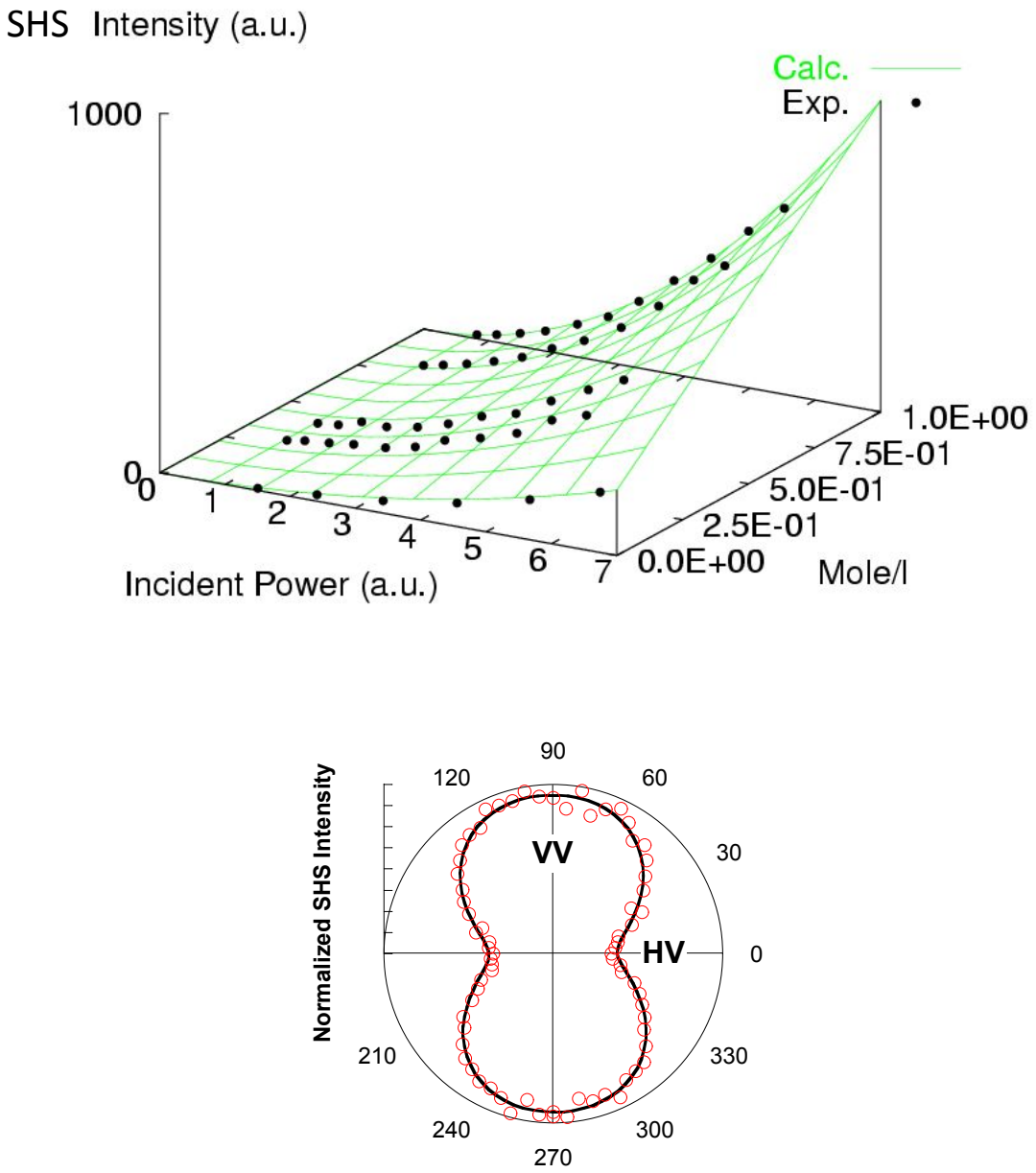

Figure S7. SHS responses of NP-4 in THF. Top: 3D representation of the SHS response as a function of the incident power and NPs concentration. Bottom: Extracted polar plot of the polarization curve of the dispersed ZnO NP-4.

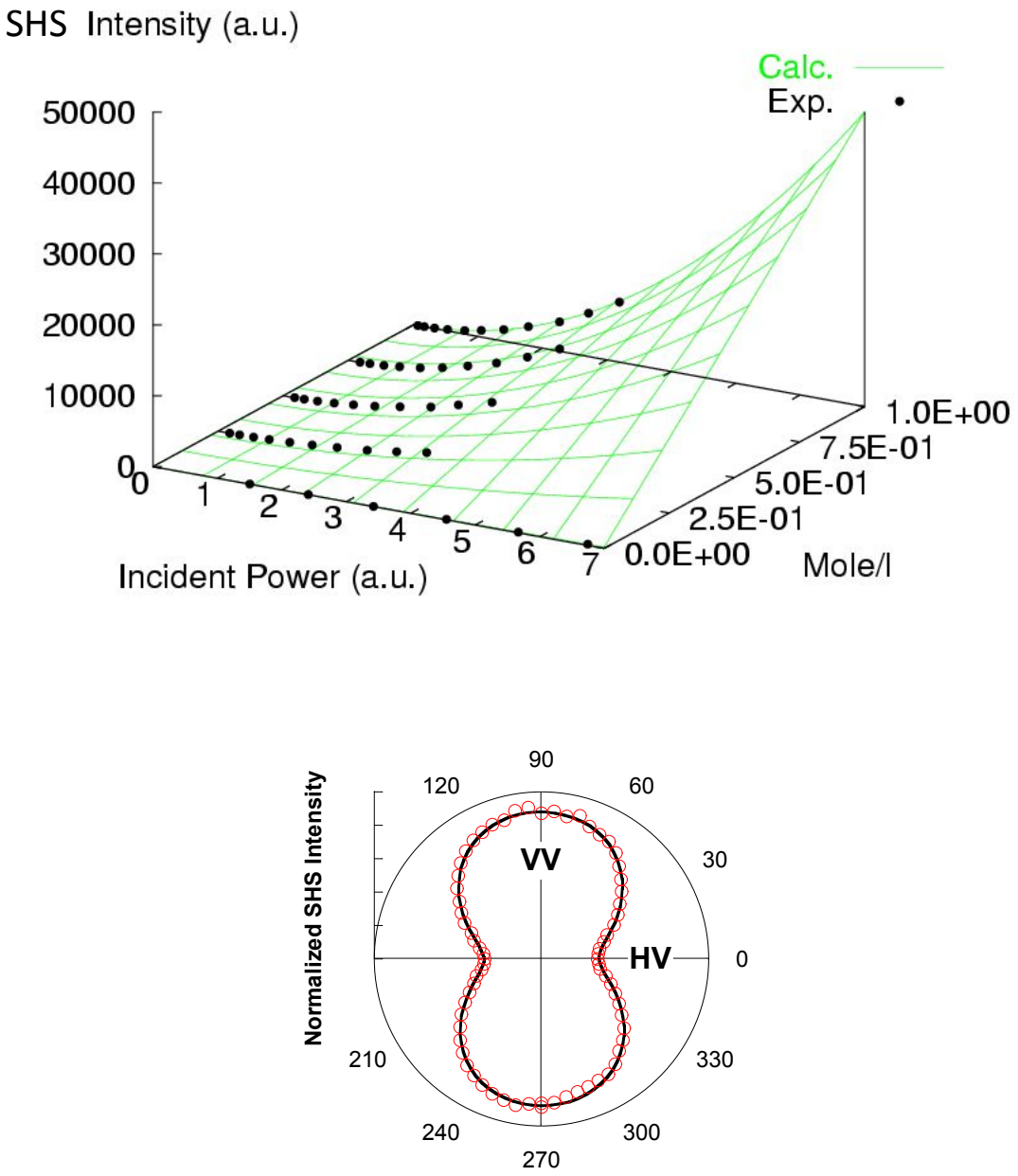

Figure S8. SHS responses of NP-5 in THF. Top: 3D representation of the SHS response as a function of the incident power and NPs concentration. Bottom: Extracted polar plot of the polarization curve of the dispersed ZnO NP-5.

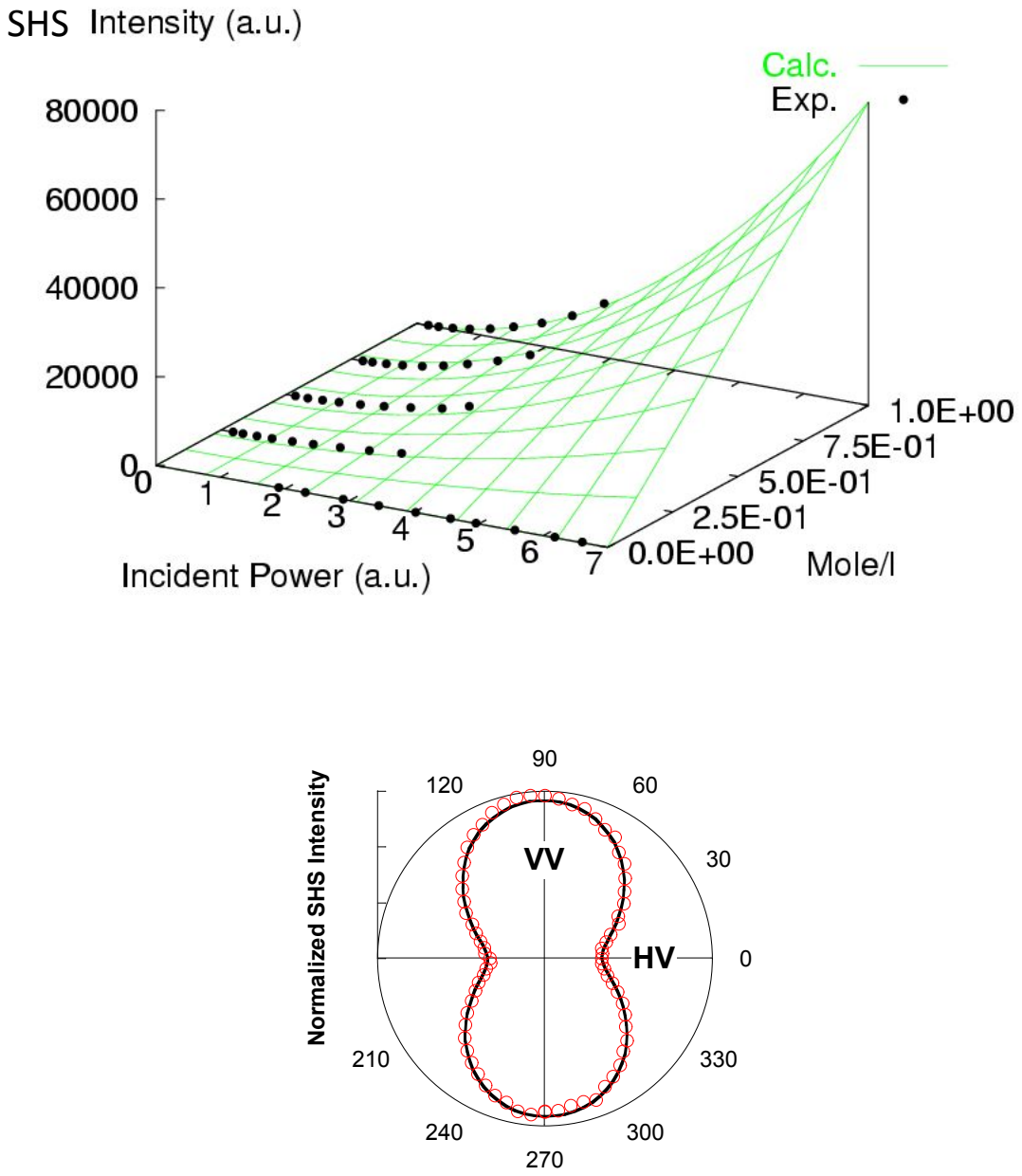

Figure S9. SHS responses of NP-6 in THF. Top: 3D representation of the SHS response as a function of the incident power and NPs concentration. Bottom: Extracted polar plot of the polarization curve of the dispersed ZnO NP-6.

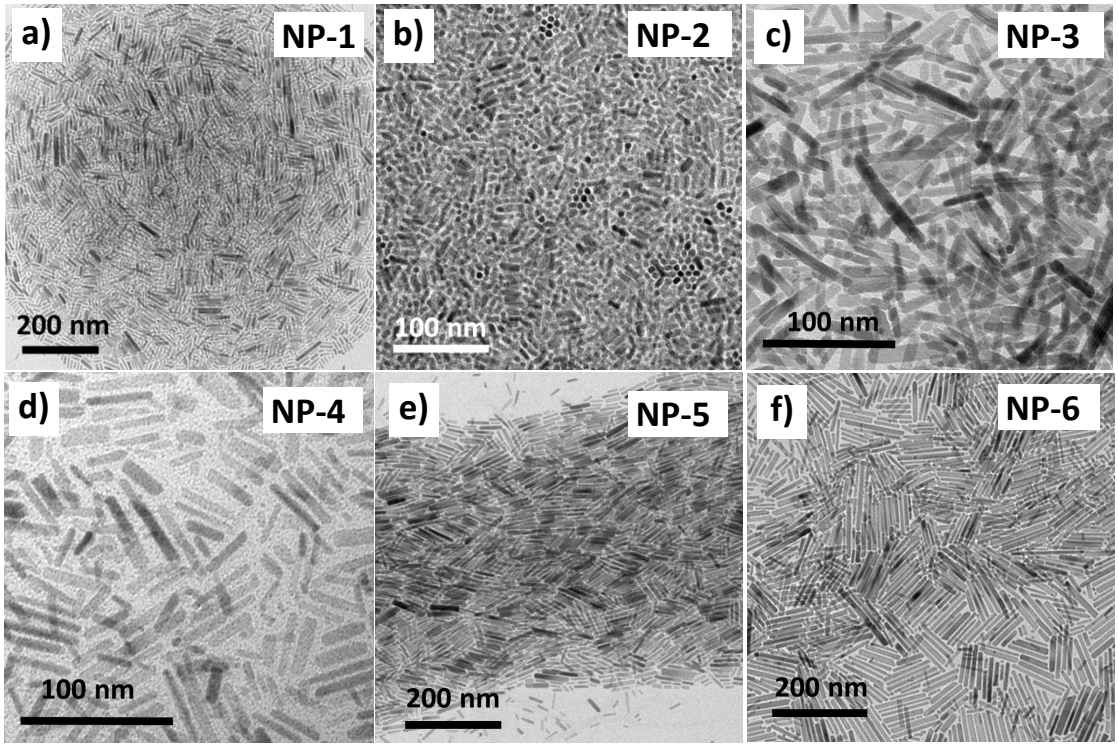

Figure S10.TEM images from a THF dispersion of ZnO nanorods prepared in the presence of methoxy-PEGamine750 a) ρ = 2, 40 ºC; b) ρ = 1.5, 40 ºC; c) ρ = 0.1, 40 ºC; d) ρ = 2, RT; e) ρ = 1, 40 ºC; and f) ρ = 0.5, 40 ºC.

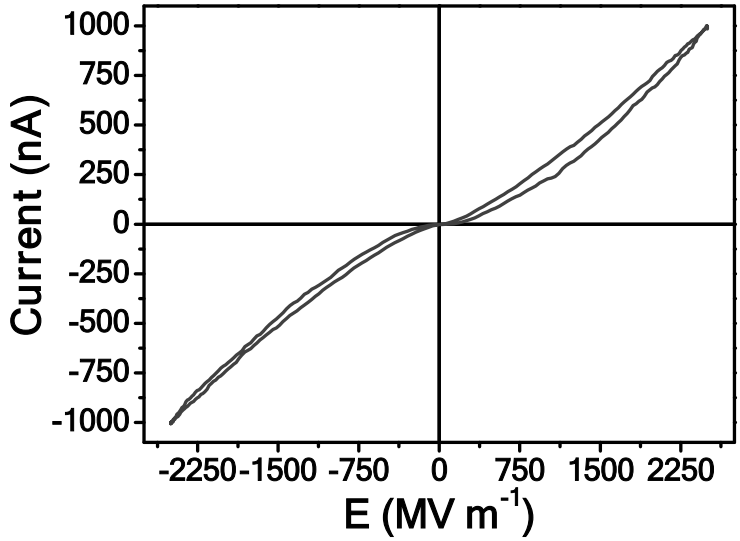

Figure S11. *I vs E* behavior of the NP-1 ZnO:PMMA blend film. Similar curves have been recorded for the NP-2 and NP-3 nanorods.

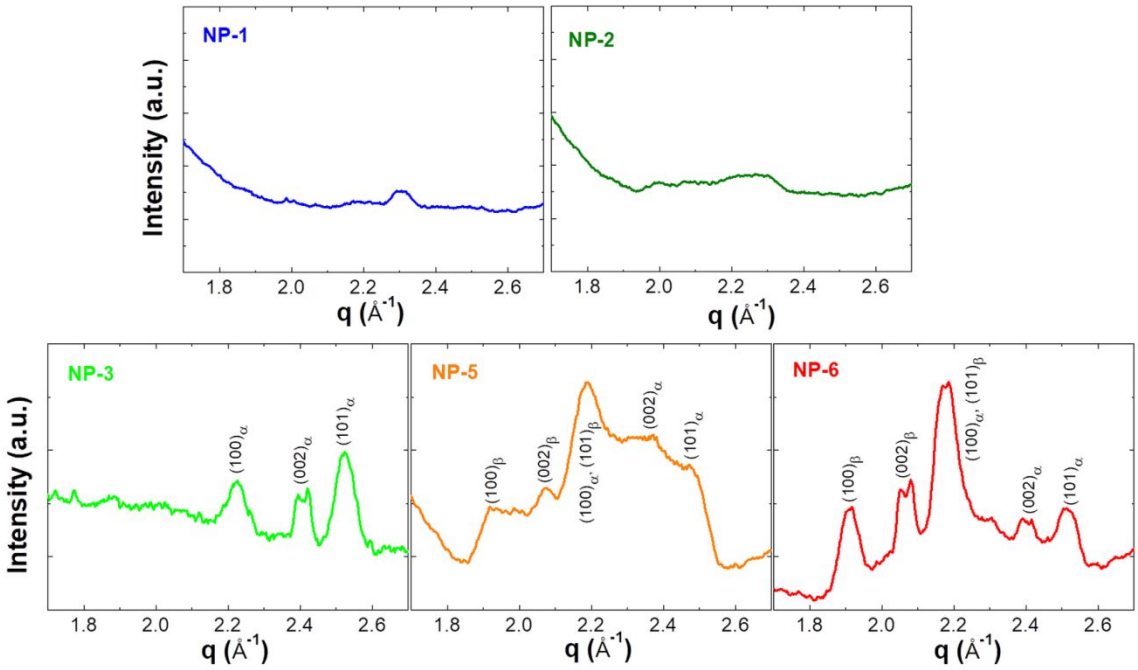

Figure S12. 1D scattering profiles for the various ZnO NPs dispersed in PMMA films. Only the q-range where the ZnO diffraction peaks arise is presented, along with the peaks indexes. The emergence of the *β* ZnO phase is shown.

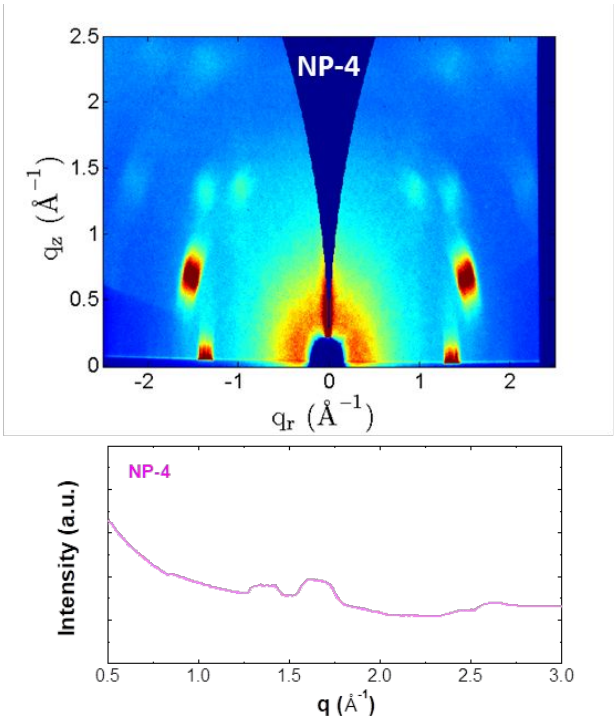

Figure S13. 2D GIWAXS image and the corresponding 1D scattering profiles for the NP-4 sample.

Discussion on Figure S13

The NP-4 ZnO nanoparticles exhibit a scattering behavior that is qualitative similar to that of NP-5. The scattering image presented in Figure S5 shows two families of spots, which we attribute to two different crystalline phases, in consistence to what has been observed for NP-5 and NP-6. The inner structure of these spots cannot be resolved (see Intensity *versus* q plot in Figure S4), therefore we cannot estimate the lattice parameters. However, the two families are centered at 1.35 $Å^{-1}$ and at 1.65 $Å^{-1}$ respectively, which suggests that the lattice parameters of these two phases are larger than those of phases α and β observed for NP-5 and NP-6. Given that synthesis of NP-4 was performed at room temperature while NP-5 and NP-6 were synthesized at 40℃, no justification of this lattice difference is attempted herein. The role of temperature on the NPs characteristics is highlighted. Similarly to the discussion on sample NP-5, the spot position at specific angles is indicative of a preferential orientation of the crystallites with respect to the substrate and of a tied orientational relationship between the two phases. It is noted that this sample was measured at BM26 at the ESRF, but during a different beamtime. The energy of the X-rays was 12 keV, the sample-to-detector distance was 12.3cm (which explains the narrower q-range explored) and the angle of incidence, α_i, was 0.15°.

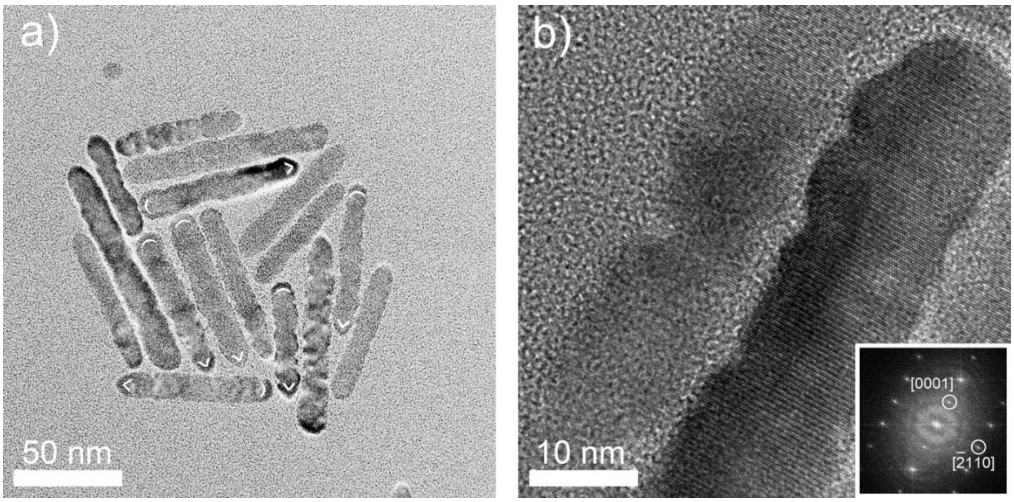

Figure S14. HRTEM micrographs of the NP-6 sample. Figure a) highlights the basal planes of the nanorods (showed with "(" and ">" marks), while b) witnesses the monocrystalline nature of the nanorods, as also confirmed by the corresponding digital diffractogram (inset).